2014 IEEE/RSJ International Conference on
Intelligent Robots and Systems (IROS 2014)
September 14-18, 2014, Chicago, IL, USA

Frequency-Domain Flight Dynamics Model Identification of MAVs - Miniature Quad-Rotor Aerial Vehicles

Guowei Cai, Hind Al Mehairi, Hanan Al-Hosani, Jorge Dias, Lakmal Seneviratne[1]

Abstract— **In this paper, a complete system identification process for identifying flight dynamics model of MAVs (miniature aerial vehicles) is presented. CIFER identification toolkit, which is developed by NASA Ames research center and particularly suitable for identifying rotary-wing aircraft dynamics, is adopted. The modeling procedure is detailed by addressing the following four key steps: 1) data collection and processing based on frequency-sweep input form, 2) parameter identification in frequency domain by minimizing the cost function, 3) result analysis based on the frequency responses matching, the Cramer-Rao Bound, and the Insensitivity, and 4) model fidelity validation in time domain.**

I. INTRODUCTION

The prevalence of miniature aerial vehicles has increased significantly over the past several decades. To date, for either miniature fixed-wing or rotary-wing aircraft, one can easily find many applications in both defense and civil communities. Various unique advantages of miniature aerial vehicles, such as low cost, small size, good maneuverability, and unique flexibility, have recently ignited a strong interest in the academic world. A lot of research effort in the associated areas (see, for example, in obstacle avoidance [8], mission planning [4], [10], trajectory management [9], vision-based surveillance [7], and etc.) have been explored and documented in the literature. At the Khalifa University Robotics Institute, we have carried out the research on miniature rotorcraft vehicles and constructed a group of quad-rotor platforms (one example is shown in Fig. 1). To achieve autonomous control, navigation, and multiple-vehicle cooperation, we have first conducted a comprehensive modeling work to obtain an accurate flight dynamics model, which is the primary focus of this paper.

An accurate flight dynamics model is compulsory if one intends to use MIMO-system-oriented control techniques to design flight control law (see, for example, [2], [3]). The necessity for modeling a quad-rotor vehicle dynamics has been seen in the documented research results such as [1], [5], [6]. There are basically two main modeling approaches available for our usage: 1) first-principles modeling that derives the flight dynamics model based on the well-established aircraft or rotorcraft theories, and 2) system identification that extracts the dynamics model using the practical input-output data collected from particular experiments. The former is generally labor intensive, and requires a lot of effort on the estimation or measurement of many elements such as the aerodynamic, inertial, and structural properties [11], whereas the latter directly relies on the real flight data and delivers the dynamics model in a more efficient and rapid way with generally enhanced physical understanding. In the work to be presented, the system identification approach is adopted to derive the flight dynamics model for our quad-rotor vehicles.

Among a number of available system identification toolkits, CIFER is utilized in our work to achieve this aim. CIFER stands for *Comprehensive Identification from FrEquency Rsponses*. It was originally developed by NASA Ames Research Center and has been extensively applied to a wide range of manned and unmanned fixed-wing and rotary-wing aircrafts during the past more than twenty years. The biggest feature or advantage of CIFER is that the model identification is conducted in the frequency domain, which is particularly suitable for the system with weakly stable or unstable dynamics mode like rotorcraft. Other associated features of CIFER include automatic noise-signal separation, less amount of involved identification data points, independent evaluation of system excitation, and etc. It is due to these advantages that we select CIFER as the identification tool.

Fig. 1. Quad-rotor aerial vehicle developed at the Khalifa University

The remaining content of this paper is organized as follows: in Section II, a flight dynamics model which contains both the six-degree-of-freedom (6DOF) rigid-body dynamics and the onboard stabilizer dynamics is first proposed. Next, in Section III, the complete identification procedure using CIFER, which starts with the data processing, followed by the frequency-domain parameter identification and result analysis, and ends with a comprehensive model fidelity validation, is presented. Finally, in Section IV, we draw some concluding remarks.

[1]Guowei Cai, Hind Al Mehairi, Hanan Al-Hosani, Jorge Dias, and Lakmal Seneviratne are with the Robotics Institute, Khalifa University, Abu Dhabi, United Arab Emirates guowei.cai, 100020268, 100020263, jorge.dias, lakmal.seneviratne@kustar.ac.ae

TABLE I

DEFINITIONS OF MODEL INPUTS AND STATES

Variable	Physical meaning
$\delta_{\mathrm{lat,d}}$	Desired roll angle input
$\delta_{\mathrm{lon,d}}$	Desired pitch angle input
$\delta_{\mathrm{col,d}}$	Desired heave velocity input
$\delta_{\mathrm{ped,d}}$	Desired yaw rate input
u, v, w	Body-frame velocities
p, q, r	Body-frame angular rates
ϕ, θ	Roll and pitch angles
e_{ai}	Intermediate state in roll angle stabilization
e_{ei}	Intermediate state in pitch angle stabilization
e_{ci}	Intermediate state in body-frame's z-axis stabilization
e_{pi}	Intermediate state in yaw rate stabilization

II. MODEL STRUCTURE OF A PARTIALLY STABILIZED QUAD-ROTOR VEHICLE

An important reason for the quad-rotor vehicles' popularity is its simplicity in physical construction: only four motors, four matched propellers, and a cross frame can form a quad-rotor vehicle properly. The resulting dynamics can be well represented by a 6DOF rigid-body equation set. However, as the coupled model-blade dynamics response is over sensitive to human pilot, a quad-rotor aerial vehicle must be equipped with an onboard stabilizer for a feasible pilot control. In what follows of this section, we introduce a model structure which is able to properly cover both aforementioned parts. The definition of its inputs and states is given in Table I.

The 6DOF rigid-body dynamics equation consists of translational and rotational parts. It is linearized at the operation point of interest (the hovering condition for this work) and expressed by

$$\begin{cases} \dot{u} = (-w_0 q - q_0 w + v_0 r + r_0 v) + \Delta X/m \\ \dot{v} = (-u_0 r - r_0 u + w_0 p + p_0 w) + \Delta Y/m \\ \dot{w} = (-v_0 p - p_0 v + u_0 q + q_0 u) + \Delta Z/m \end{cases} \tag{1}$$

and

$$\begin{cases} \dot{p} = (-q_0 r - r_0 q)(I_{\mathrm{yy}} - I_{\mathrm{zz}})/I_{\mathrm{xx}} + \Delta L/I_{\mathrm{xx}} \\ \dot{q} = (-p_0 r - r_0 p)(I_{\mathrm{zz}} - I_{\mathrm{xx}})/I_{\mathrm{xx}} + \Delta M/I_{\mathrm{yy}} \\ \dot{r} = (-p_0 q - q_0 p)(I_{\mathrm{xx}} - I_{\mathrm{yy}})/I_{\mathrm{xx}} + \Delta N/I_{\mathrm{zz}} \\ \dot{\phi} = p \\ \dot{\theta} = q \end{cases} \tag{2}$$

where u_0, v_0, w_0, p_0, q_0, and r_0 are the trimmed values, m is the mass of the vehicle, I_{xx}, I_{yy}, and I_{zz} are the moment of inertia along the three body-frame axes, ϕ and θ can be approximately treated as the integration of on-axis angular rates p and q, the $\Delta X/Y/Z$ and $\Delta L/M/N$ are the external forces and moments, respectively. They can be further expressed using a simplified Taylor series (only first-order terms are reserved) as follows

$$\begin{cases} \Delta X/m = X_u u + X_\theta \theta + X_q q \\ \Delta Y/m = Y_v v + Y_\phi \phi + Y_p p \\ \Delta Z/m = Z_w w + Z_{\mathrm{col}} \delta_{\mathrm{col}} \end{cases} \tag{3}$$

and

$$\begin{cases} \Delta L/I_{\mathrm{xx}} = L_u u + L_v v + L_p p + L_{\mathrm{lat}} \delta_{\mathrm{lat}} \\ \Delta M/I_{\mathrm{yy}} = M_u u + M_v v + M_q q + M_{\mathrm{lon}} \delta_{\mathrm{lon}} \\ \Delta N/I_{\mathrm{zz}} = N_r r + N_{\mathrm{ped}} \delta_{\mathrm{ped}} \end{cases} \tag{4}$$

Note that the above Taylor series have been simplified by omitting the stability and control derivatives that have weak effect in the corresponding dynamic mode. The elimination of these derivatives is determined by the frequency responses selection result, which is to be addressed in Section III-B. The δ_{lat}, δ_{lon}, δ_{col}, and δ_{ped} are the aileron, elevator, throttle, and rudder input following the convention of the fixed-wing aircraft operation principle. Due to the existence of the onboard stabilizer, they are just intermediate states and will be replaced by the following equations related to the stabilizer dynamics. Correspondingly, the actual inputs of the following state-space model are denoted by $\delta_{\mathrm{lat,d}}$, $\delta_{\mathrm{lon,d}}$, $\delta_{\mathrm{col,d}}$, and $\delta_{\mathrm{ped,d}}$, as shown in Table I.

To assist pilot control, a factory-installed onboard stabilizer module, which provides additional damping for roll angle ϕ, pitch angle θ, body-frame velocity w, and yaw rate r, is employed. For the rolling and pitching motion, both angle (ϕ or θ) and angular rate (p or q) are fed back into the stabilizer, and the classic PID control technique is adopted to achieve the stabilization. As for w and r, only one state can be used for feedback. To hold the validity of the state-space dynamics model, PI controller is adopted to represent the stabilization procedure. Four intermediate states e_{ai}, e_{ei}, e_{ci}, and e_{pi}, as denoted before in Table I, are defined and the onboard stabilizer dynamics are expressed by

$$\begin{cases} \dot{e}_{\mathrm{ai}} = K_{\mathrm{aa}} \delta_{\mathrm{lat,d}} - \phi \\ \delta_{\mathrm{lat}} = K_{\mathrm{Pa}}(K_{\mathrm{aa}} \delta_{\mathrm{lat,d}} - \phi) + K_{\mathrm{Ia}}\, e_{\mathrm{ai}} + K_{\mathrm{Da}} p \end{cases} \tag{5}$$

$$\begin{cases} \dot{e}_{\mathrm{ei}} = K_{\mathrm{ae}} \delta_{\mathrm{lon,d}} - \theta \\ \delta_{\mathrm{lon}} = K_{\mathrm{Pe}}(K_{\mathrm{ae}} \delta_{\mathrm{lon,d}} - \theta) + K_{\mathrm{Ie}}\, e_{\mathrm{ei}} + K_{\mathrm{De}} q \end{cases} \tag{6}$$

$$\begin{cases} \dot{e}_{\mathrm{ci}} = K_{\mathrm{ac}} \delta_{\mathrm{col,d}} - w \\ \delta_{\mathrm{col}} = K_{\mathrm{Pc}}(K_{\mathrm{ac}} \delta_{\mathrm{col,d}} - w) + K_{\mathrm{Ic}}\, e_{\mathrm{ci}} \end{cases} \tag{7}$$

$$\begin{cases} \dot{e}_{\mathrm{pi}} = K_{\mathrm{ap}} \delta_{\mathrm{ped,d}} - r \\ \delta_{\mathrm{ped}} = K_{\mathrm{Pp}}(K_{\mathrm{ap}} \delta_{\mathrm{ped,d}} - r) + K_{\mathrm{Ip}}\, e_{\mathrm{pi}} \end{cases} \tag{8}$$

By integrating the 6DOF rigid-body dynamics with the onboard stabilizer dynamics, a complete state-space dynamics model for our quad-rotor vehicle can be established as follows

$$\dot{x} = \boldsymbol{A}x + \boldsymbol{B}u \tag{9}$$

where

$$x = [\, u \quad v \quad \phi \quad p \quad e_{\mathrm{ai}} \quad \theta \quad q \quad e_{\mathrm{ei}} \quad w \quad e_{\mathrm{ci}} \quad r \quad e_{\mathrm{pi}} \,], \tag{10}$$

$$u = [\, \delta_{\mathrm{lat,d}} \quad \delta_{\mathrm{lon,d}} \quad \delta_{\mathrm{col,d}} \quad \delta_{\mathrm{ped,d}} \,], \tag{11}$$

Note that * in (12) denotes the difference of the associated parameters compared with the counterparts appearing in (3) and (4). Indeed, they are lumped parameters that integrate both the aforementioned bare quadcopter dynamics and stabilizer dynamics.

$$\boldsymbol{A}=\begin{bmatrix} X_u & 0 & 0 & 0 & 0 & X_\theta & X_q & 0 & 0 & 0 & 0 & 0 \\ 0 & Y_v & Y_\phi & Y_p & 0 & 0 & 0 & 0 & 0 & 0 & 0 & 0 \\ 0 & 0 & 0 & 1 & 0 & 0 & 0 & 0 & 0 & 0 & 0 & 0 \\ L_u & L_v & L_\phi^* & L_p^* & L_e^* & 0 & 0 & 0 & 0 & 0 & 0 & 0 \\ 0 & 0 & -1 & 0 & 0 & 0 & 0 & 0 & 0 & 0 & 0 & 0 \\ 0 & 0 & 0 & 0 & 0 & 0 & 1 & 0 & 0 & 0 & 0 & 0 \\ M_u & M_v & 0 & 0 & 0 & M_\theta^* & M_q^* & M_e^* & 0 & 0 & 0 & 0 \\ 0 & 0 & 0 & 0 & 0 & -1 & 0 & 0 & 0 & 0 & 0 & 0 \\ 0 & 0 & 0 & 0 & 0 & 0 & 0 & 0 & Z_w^* & Z_e^* & 0 & 0 \\ 0 & 0 & 0 & 0 & 0 & 0 & 0 & 0 & -1 & 0 & 0 & 0 \\ 0 & 0 & 0 & 0 & 0 & 0 & 0 & 0 & 0 & 0 & N_r^* & N_e^* \\ 0 & 0 & 0 & 0 & 0 & 0 & 0 & 0 & 0 & 0 & -1 & 0 \end{bmatrix}, \quad \boldsymbol{B}=\begin{bmatrix} 0 & 0 & 0 & 0 \\ 0 & 0 & 0 & 0 \\ 0 & 0 & 0 & 0 \\ L_{\text{lat}}^* & 0 & 0 & 0 \\ K_{\text{alat}} & 0 & 0 & 0 \\ 0 & 0 & 0 & 0 \\ 0 & M_{\text{lon}}^* & 0 & 0 \\ 0 & K_{\text{alon}} & 0 & 0 \\ 0 & 0 & Z_{\text{col}}^* & 0 \\ 0 & 0 & K_{\text{acol}} & 0 \\ 0 & 0 & 0 & N_{\text{ped}}^* \\ 0 & 0 & 0 & K_{\text{aped}} \end{bmatrix} \tag{12}$$

III. CIFER-Based Parameter Identification

In this section, the CIFER-based parameter identificatio procedure is detailed. Generally it consists of four key steps 1) data collection and processing, 2) model-wise paramete identification, 3) identified results analysis, and 4) mode fidelity validation.

A. Data Collection and Processing

In this step, a series of experiments are first conducte The input and output data collected are further converted into the frequency domain for the parameter identification usage. As for time-domain data collection, frequency sweep is adopted as the input signal. The frequency sweep refers to a class of control inputs that has a quasi-sinusoidal shape of increasing frequency [11]. During the experiments, the quad-rotor vehicle starts with an ideal hover at an altitude of 5 m to avoid ground effect. With the onboard stabilizer functioning, the frequency sweep, which is issued by an experienced pilot through a wireless radio-control joystick, is then sequentially injected into one of the four input channels (that is, $\delta_{\text{lat,d}}$, $\delta_{\text{lon,d}}$, $\delta_{\text{col,d}}$, and $\delta_{\text{ped,d}}$) to persistently excite the flight dynamics of the quad-rotor vehicle over the frequency range of interest. While conducting the frequency sweep in one channel, the pilot needs to maintain the hover condition but is required to issue minimum and uncorrelated control signals in the remaining input channels. Once a perturbation is complete, the quad-rotor vehicle needs to retrieve the ideal hover condition before the signal recording for both inputs and outputs is stopped. Such data collection procedure is applied to each input channel and repeated for a number of times (normally 3-5 times) to ensure sufficient high-quality data have been collected. In Fig. 2, an example of the frequency sweep issued in the channel $\delta_{\text{lat,d}}$, together with the on-axis roll rate and angle responses (p and ϕ), is shown for illustration.

In data processing, the following three main tasks are sequentially completed:

1) Individual input-output data are first converted from time domain to frequency domain. Next, checking on data quality and consistency is conducted to ensure that only high-qualify data are included and then merged for the subsequent parameter identification. For the former, the coherence function estimate γ_{xy}^2, which is defined below and indicates whether the system being modeled is well characterized as a linear process in the frequency range of interest [11], is adopted as the evaluation index. For the latter, different frequency-domain responses are overlapped together and the corrupted ones can be easily picked out based on visual observation.
$$\gamma_{xy}^2=\frac{|G_{xy}|^2}{|G_{xx}||G_{yy}|} \tag{13}$$
where G_{xx}, G_{yy}, and G_{xy} stand for input auto-spectrum, output auto-spectrum, and cross spectrum, respectively.
2) The previous step generates a series of single-input/single-output (SISO) data set. This database is further red by CIFER and conditioned such that the effects of multiple, partially correlated controls that might have been present in the record can be removed [11].
3) Next, CIFER performs an optimization across the multiple spectral windows to achieve a final frequency-response database with good resolution, broad bandwidth, and low random error [11].

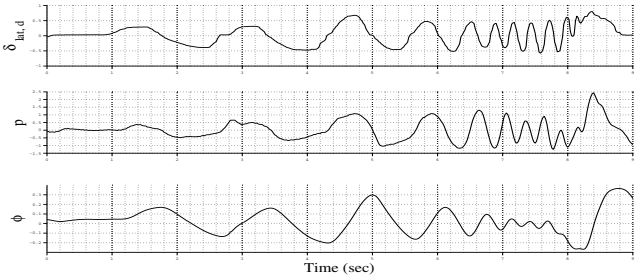

Fig. 2. Frequency sweep issued in channel $\delta_{\text{lat,d}}$ and the on-axis responses

In CIFER, three sub-programmes, named FRESPID, MISOSA, and COMPOSITE, are utilized to achieve these three tasks respectively. After these processing, a $4 * 8$ pair-wise multi-input/multi-output (MIMO) frequency-response database, as shown in Table II, is created for parameter identification. Note that for the output side, the four inter-

TABLE II

FREQUENCY RESPONSES SELECTION FOR PARAMETER IDENTIFICATION

	u	v	ϕ	p	θ	q	w	r
$\delta_{\mathrm{lat,d}}$		*	*	*				
$\delta_{\mathrm{lon,d}}$	*				*	*		
$\delta_{\mathrm{col,d}}$							*	
$\delta_{\mathrm{ped,d}}$								*

mediate states custom-defined in Table I are not included. Fig. 3 shows the frequency responses (from $\delta_{\mathrm{lat,d}}$ to ϕ) converted from two time histories. Both the closed matching and the high coherence values over the entire frequency range indicate their high quality.

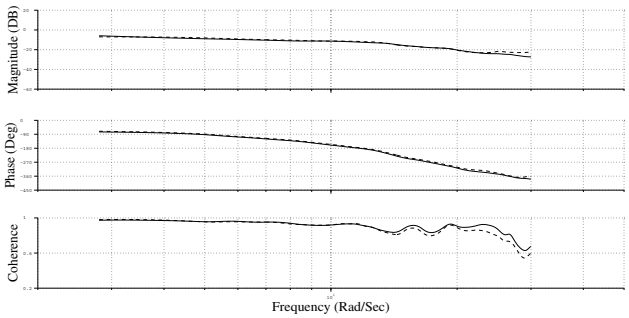

Fig. 3. Comparison of two frequency responses from $\delta_{\mathrm{lat,d}}$ to ϕ

B. Mode-Wise Parameter Identification

The identification of a MIMO system such as a quadrotor vehicle dynamics is a challenging topic due to the high order (12 for our case) and the large amount of parameters involved. An efficient way to substantially reduce the complexity of the identification procedure is to check the the correlation of each input-output pair and just include the data as well as the parameters that are essential to reflect the system dynamics. To achieve this aim, each data set of $4*8$ frequency responses database is examined by checking its associated coherence function estimate. According to [11], only the data with coherence value higher than 0.6 has the necessity to be included in the identification process, and the result is shown in Table II. It can be noted that, due to the existence of the onboard stabilizer, only the on-axis (e.g., from $\delta_{\mathrm{lat,d}}$ to v, ϕ, and p) frequency responses need to be included. As a result, the model structure can be greatly simplified to the format given in (12) by omitting most of the parameters that are related to off-axis dynamics, and the overall identification issue can be further decoupled into three primary modes: 1) the coupled longitudinal-lateral dynamics mode, 2) the heave dynamics mode, and 3) the yaw dynamics mode.

For each of the three modes, the identification programme in CIFER, named DERIVED, starts with selecting the effective frequency range in which the coherence value is higher than 0.6. The complete range selection is provided in Table III. The initial values for the parameters to be identified

TABLE III

FREQUENCY RANGE SELECTION

Frequency responses	Frequency range (rad/sec)
$\delta_{\mathrm{lat,d}}$ to v	$2.8 \sim 8.5$
$\delta_{\mathrm{lat,d}}$ to ϕ	$2.8 \sim 24$
$\delta_{\mathrm{lat,d}}$ to p	$2.8 \sim 24$
$\delta_{\mathrm{lon,d}}$ to u	$2.2 \sim 7.4$
$\delta_{\mathrm{lon,d}}$ to θ	$1.8 \sim 26$
$\delta_{\mathrm{lon,d}}$ to q	$1.8 \sim 26$
$\delta_{\mathrm{col,d}}$ to w	$1.5 \sim 12$
$\delta_{\mathrm{ped,d}}$ to r	$2.1 \sim 15$

are determined based on the first-principles flight dynamics analysis. In the meantime, a series of transfer functions ($l = 1$ to n_{TF}) for the selected input-output frequency responses marked in Table II are created. The iterative parameter tuning process is resolved by minimizing the cost function defined in (14), in which the differences of both magnitude and phase angle ($\Delta|T|$ and $\Delta\angle T$) over the selected frequency range (from ω_1 to ω_{n_ω}) are weighted and taken into account.

$$J = \sum_{l=1}^{n_{\mathrm{TF}}} \left\{ \frac{20}{n_\omega} \sum_{\omega_1}^{\omega_{n_\omega}} W_\gamma \left[W_{\mathrm{g}} (\Delta|T|)^2 + W_{\mathrm{p}} (\Delta\angle T)^2 \right] \right\}_l \tag{14}$$

The average cost function is further defined as follows

$$J_{\mathrm{ave}} = \frac{J}{n_{\mathrm{TF}}}, \tag{15}$$

and $J_{\mathrm{ave}} \leq 100$ denotes that sufficient accuracy of the involved parameters has been obtained and the identification progress can be terminated. Finally, Table IV provides the complete list of the identified parameters after running the DERIVED programme. Note that the four parameters with † (i.e., X_θ, Y_ϕ, L_u, and M_v) have their values fixed to the first-principles modeling analysis to further simplify the parameter identification process.

C. Identified Result Analysis

CIFER provides the following three ways to comprehensively evaluate the identified results: 1) frequency responses matching, 2) Cramer-Rao Bound, and 3) Insensitivity.

Examining the matching of the frequency responses is the most direct and native way to evaluate the accuracy of the identified parameters. Fig. 4 gives the final frequency matching comparison results for our identification work, in which all the key on-axis dynamics (e.g., $\delta_{lat,d}$ to v and p, $\delta_{lon,d}$ to u and q, $\delta_{col,d}$ to w and $\delta_{ped,d}$ to r are displayed. One can easily observe that for each of the listed dynamic mode, the CIFER-generated frequency response (the dashed line) overlaps the actual counterpart (solid line) closely over the entire frequency range, which indicate the identified model holds sufficient accuracy. Frequency response matching is actually the visual reflection of the cost function defined in (14). Such visualization provides us a more straightforward way to observe the discrepancy during the identification process and conduct further refinement.

Besides frequency responses matching, another two quantitative evaluation indices, that is, the Cramer-Rao Bound

TABLE IV

PARAMETERS IDENTIFIED IN CIFER WITH THE CR BOUND AND INSENSITIVITY VALUES

Derivative	Value	CR Bound(%)	Insens (%)
X_u	-0.19	33.89	7.01
X_θ	-9.8†	NA	NA
X_q	-10.35	10.75	5.51
Y_v	-0.17	32.29	6.31
Y_ϕ	9.8†	NA	NA
Y_p	-11.22	11.77	4.55
L_u	0†	NA	NA
L_v	0.11	6.15	10.25
L_ϕ^*	-223.08	18.74	2.04
L_p^*	-34.07	18.77	2.15
L_e^*	557.69	18.74	2.04
M_u	-0.39	12.93	14.51
M_v	0†	NA	NA
M_θ^*	-221.58	10.58	2.32
M_q^*	-33.64	10.34	2.46
M_e^*	553.95	10.58	2.32
Z_w^*	-14.06	17.39	2.86
Z_e^*	58.18	14.50	2.41
N_r^*	-8.94	19.11	2.24
N_e^*	17.58	16.21	1.96
L_{lat}^*	74.48	18.74	2.04
K_{alat}	0.33	5.08	1.88
M_{lon}^*	77.02	10.58	2.32
K_{alon}	0.35	4.56	1.91
Z_{col}^*	-162.66	14.50	2.41
K_{acol}	-7.13	6.72	2.07
N_{ped}^*	28.51	16.21	1.96
K_{aped}	-3.78	10.01	1.96

expressed in percentage (CR Bound), and the Insensitivity (Insens) expressed in percentage, can be utilized to examine the reliability of each individual parameter that needs to be identified. More specifically, the Cramer-Rao Bound value indicates the identifiability of the parameter of concern and suggests whether this parameter should be eliminated (or fixed) in the model structure [11], and the Insensitivity value reveals the correlation between the parameter and the converged cost function. In other words, it indicates whether the parameter is important to the determined model structure [11]. The general guidelines for the Cramer-Rao Bound and the Insensitivity are

$$\begin{cases} \text{CR Bound} \leq 20\% \\ \text{Insens} < 10\% \end{cases} \tag{16}$$

For our work, the CR Bound and Insensitivity values for all the involved parameters are provided in Table IV. It can be observed that the majority of the parameters satisfies the above guidelines, indicating that they are both compulsory to the model structure proposed in Section II and can be identified with sufficient accuracy and reliability. Four parameters (i.e., X_u, Y_v, L_v, and M_u) have the CR Bound or Insens values exceeding the guidelines, which is mainly due to the insufficient data in the low frequency range (less than 1.5 rad/sec). This shortcoming can be overcome by including more high-quality identification data.

D. Model Fidelity Validation

Model fidelity validation is carried out in the time domain. As suggested in [11], the roughly symmetric doublet, which is shown in Fig. 5 and includes both transient and short-period steady maneuvering, is selected as the input. Similar to the data collection experiment, the doublet input is also issued manually through a joystick and injected into each of the four input channels sequentially. Both the input and the resulting output responses are recorded. The identical input sequence is then applied to the identified model to generate the model responses in CIFER. The fidelity is examined by comparing the model-generated responses with the actual ones. Figs. 6 and 7 show the four doublet inputs together with the associated on-axis responses. It can be easily observed that for each of the outputs displayed, the model response matches the practical data very closely, indicating the sufficient robustness and accuracy of the identified model.

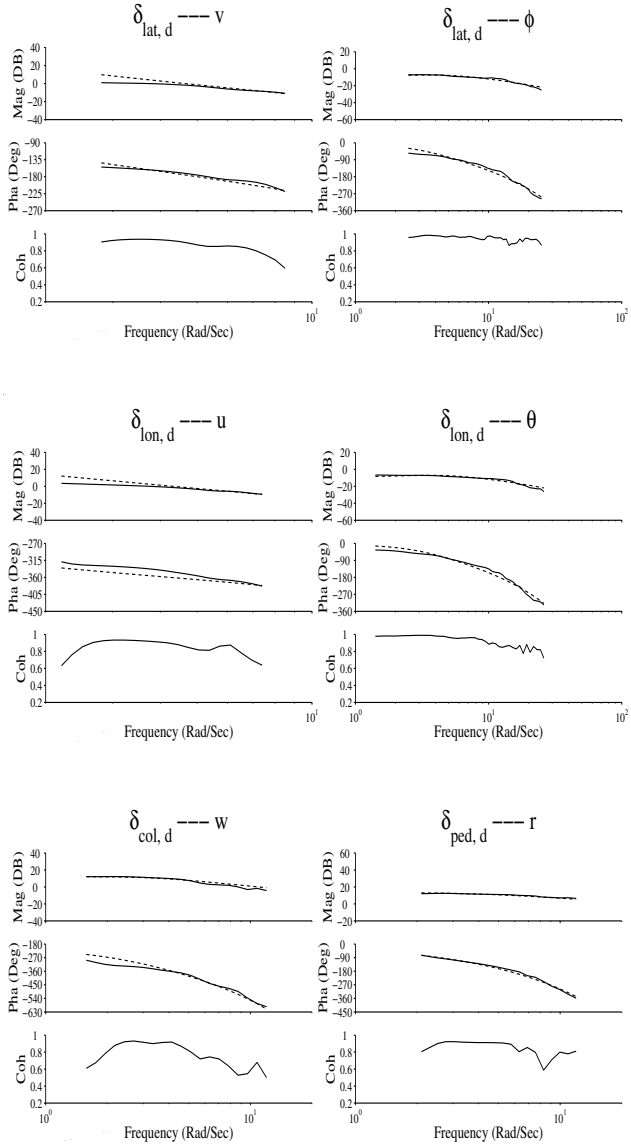

Fig. 4. Frequency responses matching examination

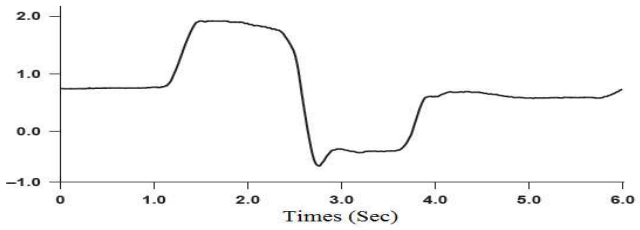

Fig. 5. Roughly symmetric doublet input

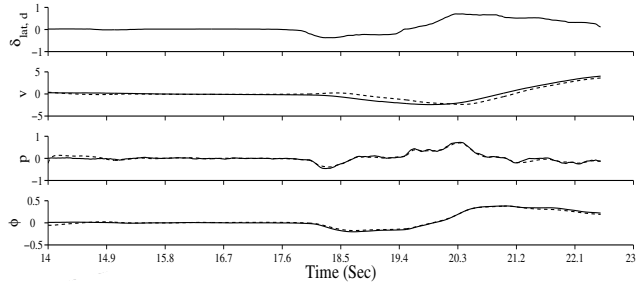

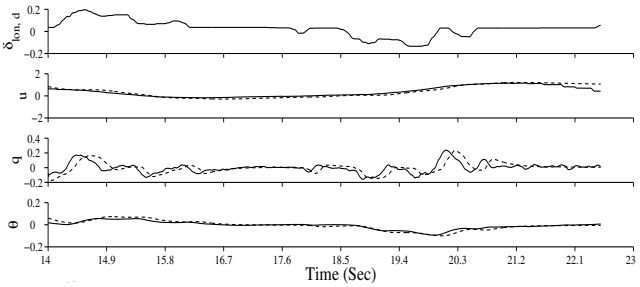

Fig. 6. Verification result for $\delta_{\mathrm{lat,d}}$ and $\delta_{\mathrm{lon,d}}$ doublet input

IV. Conclusion

A number of key conclusions of our CIFER-based modeling work can be drawn as follows:

1) A suitable flight dynamics model has developed by coupling the classic 6DOF rigid-body dynamics with the onboard PI- or PID-based stabilizer dynamics.
2) The professional identification toolkit CIFER is able to identify the proposed quad-rotor vehicle model rapidly and efficiently.
3) Besides the time-domain model validation, in CIFER one can use frequency response matching, Cramer-Rao Bound, and Insensitivity to evaluate the accuracy of any individual parameter or frequency response, which maximizes the identification accuracy.
4) The inconsistency of the frequency response matching in some frequency slots is mainly due to the insufficiency of the information contained in the raw time-history data. In an ongoing work, more qualified data have been added to the current database and we are intending to further enhance the model accuracy across an extended frequency range.

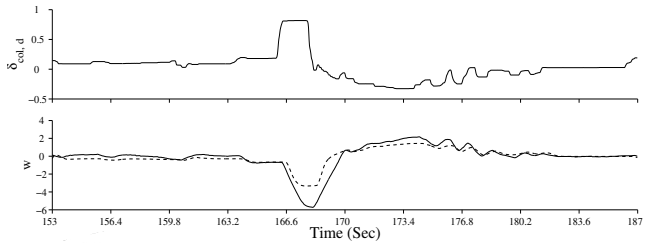

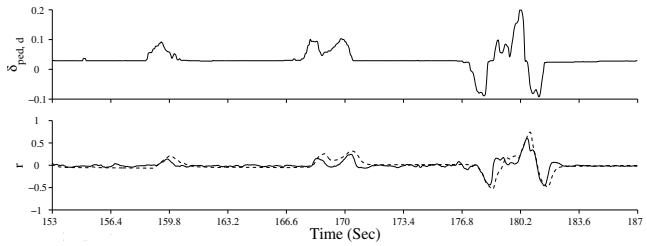

Fig. 7. Verification result for $\delta_{\mathrm{col,d}}$ and $\delta_{\mathrm{ped,d}}$ doublet input

References

[1] P. J. Bristeau, P. Martin, E. Salaun and n. Petit, "The role of propeller aerodynamics in the model of a quadrotor UAV," *Proceedings of the European Control Conference*, pp. 683-688, Budapest, Hungary, August 2009.

[2] G. Cai, B. M. Chen and T. H. Lee, "Unmanned Rotorcraft Systems", Springer, New York, 2011 (Advances in Industrial Control Series).

[3] G. Cai, B. Wang, B. M. Chen and T. H. Lee, "Design and implementation of a flight control system for an unmanned rotorcraft using RPT control approach," *Asian Journal of Control*, Vol. 15, No. 1, pp. 95-119, January 2013.

[4] P. Hoherty, F. Heintz and J. Kvarnstrom, "High-level mission specification and planning for collaborative unmanned aircraft systems using delegation," *Unmanned Systems*, Vol. 1, No. 1, pp. 75-119, 2013.

[5] H. Huang, G. M. Hoffmann, S. L. Waslander, and C. J. Tomlin, "Aerodynamics and control of autonomous quadrotor helicopters in aggressive maneuvering," *Proceedings of the 2009 IEEE International Conference on Robotics and Automation*, pp. 3277-3282, Kobe, Japan, May 2009.

[6] K. Li, S. K. Phang, B. M. Chen and T. H. Lee, "Platform design and mathematical modeling of an ultralight quadrotor micro aerial vehicle," *Proceedings of the 2013 International Conference on Unmanned Aircraft Systems*, Atlanta, USA, pp. 1066-1075, May 2013.

[7] P. C. Niedfeldt, B. T. Carroll, J. A. Howard, R. W. Beard, B. S. Morse and S. Pledgie, "Enhanced UAS surveillance using a video utility metric," *Unmanned Systems*, Vol. 1, No. 2, pp. 277-296, 2013.

[8] K. Kang and J. V. R. Prasad, "Development and flight test evalulations of an autonomous obstacle avoidance system for a rotary-wing UAV," *Unmanned Systems*, Vol. 1, No. 1, pp. 3-19, 2013.

[9] J. Keller, D. Thakur, V. Dobrokhodov, K. Jones, M. Pivtoraiko, J. Gallier, I. Kaminer and V. Kumar, "A computationally efficient approach to trajectory management for coordinated aerial surveillance," *Unmanned Systems*, Vol. 1, No. 1, pp. 59-74, 2013.

[10] A. N. Kopeikin, S. S. Ponda, L. B. Johnson and J. P. How, "Dynamic mission planning for communication control in multiple unmanned aircraft teams," *Unmanned Systems*, Vol. 1, No. 1, pp. 41-58, 2013.

[11] M. B. Tischler and R. K. Remple, "Aircraft and rotorcraft system identification: engineering methods with flight test examples," Reston, VA: AIAA Press; 2006.